J Fluoresc (2015) 25:795–801
DOI 10.1007/s10895-015-1590-5

SHORT COMMUNICATION

Structural and Optical Properties of White Light Emitting ZnS:Mn^{2+} Nanoparticles at Different Synthesis Temperatures

K. R. Bindu [1,2] · **E. I. Anila** [2]

Received: 11 April 2015 / Accepted: 4 June 2015 / Published online: 18 June 2015

Abstract We report of the synthesis and characterisation of white emitting ZnS:Mn^{2+} nanoparticles. The spectroscopic properties and the crystal structure of Mn doped ZnS nanoparticles are studied here to provide a better understanding on how the luminescence emission and the crystalline composition are influenced by the synthesis temperature. The synthesis of the samples were carried out by the simple wet chemical precipitation method. The influence of synthesis temperature on structure and optical properties were studied at constant Mn concentration. The nanoparticles were structurally characterized by X-Ray Diffraction (XRD) and Scanning Electron Microscopy (SEM). The XRD studies show the phase singularity of Mn doped ZnS particles having zinc-blende (cubic) structure at all temperatures. The band gap of the doped samples are red shifted with temperature. Electron Paramagnetic Resonance (EPR) spectra exhibited resonance signals, characteristic of Mn^{2+}. Incorporation of Mn in the ZnS nanoparticles was confirmed by Inductively Coupled Plasma- Atomic Emission Spectroscopic studies (ICP-AES). The samples show an efficient emission of yellow–orange light centred at 590 nm which is characteristic of Mn^{2+} along with a blue emission at 435 nm due to sulfur vacancy. The overall emission is white at all temperatures with CIE co-ordinates in close agreement with achromatic white.

✉ E. I. Anila
anilaei@gmail.com

[1] Sree Sankara Vidyapeetom College, Valayanchirangara, Perumbavoor, Kerala 683556, India

[2] Optoelectronic and Nanomaterials' Research Laboratory, Department of Physics, Union Christian College, Aluva, Kerala 683102, India

Keywords Semiconductors · ZnS · Photoluminescence · Nanoparticles · Paramagnetism

Introduction

Semiconducting nano-materials have been the key drivers for the swelling interest in nano-science and technology. Nanoparticles attracted considerable attention in recent years because of their special properties, such as quantum size effects and unusual luminescence phenomenon. A reduction in the particle size strongly influences the crystallinity, ionization potential, mechanical strength, melting point and structural stability etc. The size dependent optical properties have many potential applications in the areas of solar energy conversion, light emitting devices, chemical/biological sensors, photo catalysis and optoelectronic devices [1–6]. ZnS is a II-VI compound semiconductor with direct band gap of 3.65 eV at room temperature and widely used as a phosphor in optical devices. The luminescence properties can further be tuned by incorporations of impurity atoms into the pure semiconductor lattice. This process, known as doping provides new states in the band gap region of the semiconductor and hence alternative pathways for recombination of the electron–hole pair giving rise to emission energy different from that of host semiconductors. ZnS with some impurities as activators, such as certain transition or rare-earth metals have been widely used as luminescent materials owing to their luminescent characteristics and thermal stability [7–11]. For instance, the ZnS can be doped with manganese without changing the crystallinity of the host lattice to give efficient yellow emission. To obtain high quality nano phosphors, it is essential to understand the role of both the temperature and the concentration of doping. Numerous investigations have been done to understand the effect of the concentration of Mn on the particle size and

optical characteristics of ZnS nanoparticles [12–15]. For the application of ZnS:Mn nanoparticles in visible LED, extensive research work is going on to tune its dual emission by varying the amount of Mn incorporated in ZnS, by varying the synthesis temperature and by using different organic capping agents. Hence, it is advantageous to obtain efficient, tunable PL emission from uncapped ZnS:Mn nanoparticles. However from our literature survey, it is recognized that no systematic investigations of the effect of preparation temperature on the structural and optical properties have been performed, considering the crystallinity for ZnS:Mn nanoparticles. Also reports are not observed for white emitting ZnS:Mn nanoparticles. Although various methods [16–20] are available for the synthesis of Mn^{2+} doped ZnS nanoparticles, we preferred chemical precipitation technique, to study the effect of the preparation temperature on the particle size, optical absorption and photoluminescence keeping concentration constant.

Experimental

Chemical precipitation technique used in this study has the distinct qualities such as low processing temperature (<100 °C), simplicity of processing, low cost and high rate of powder collection. Synthesis of pure ZnS nanoparticles by wet chemical method was reported by the authors previously [21]. We followed the same procedure in the synthesis of manganese doped ZnS nanoparticles. Twenty five milliliter each of zinc acetate Zn $(CH3COO)_2$, $MnCl_2$ and Na_2S solutions in water were used for the preparation of Mn^{2+} doped ZnS nanoparticles. 0.001 M solution of $MnCl_2$ was added drop wise to 1 M zinc acetate $Zn(CH_3COO)_2$ solution. One molar Na_2S solution was added drop wise with continuous stirring using magnetic stirrer. The solution was stirred for 20 min keeping temperature constant. The resulting white colloidal suspension was filtered, and the filtrate was washed with de-ionized water and dried by keeping in an oven at 70 °C for 1 day. Three samples were prepared at room temperature, 50 and 70 °C. To determine crystallite size and phase of the samples, x-ray diffraction spectra were obtained with Bruker AXS D8 Advance x-ray diffractometer with Cu (1.5405 A°) as X-ray source at 40 kV and 35 mA under the same conditions. The phase identification was carried out with the help of standard JCPDS database. The diffuse reflection spectroscopy were carried out on a Varian Cary 5000 UV–VIS-NIR spectrophotometer with a spectral bandwidth of 2 nm. The spectra were recorded at room temperature in the wavelength range of 220 – 2000 nm. The photoluminescence emission spectra were recorded at room temperature using Horiba Fluromax 4C research spectro fluorometer with a 150 W ozone free Xenon lamp as an excitation source of range 200–900 nm. The observation was done keeping the slit width at 5 nm and integration time 0.1 s Morphological study was carried out using scanning electron microscopy (SEM) using Jeol model JSM 6390 LV. Inductively coupled plasma (ICP) (ICP-1000IV, Shimadzu) analysis was performed to determine the chemical composition of the samples. Electron paramagnetic resonance spectra (EPR) were recorded at room temperature using a JEOL-FE1X EPR spectrometer.

Results and Discussion

XRD Study

Figure 1 shows the XRD patterns of the ZnS:Mn^{2+} nanoparticles prepared at room temperature, 50 °C &70 °C. The three peaks in XRD pattern are at the same Braggs angle(2θ) which could be indexed to scattering from (111), (220) and (311) planes of the cubic phase ZnS nanoparticles corresponding to JCPDS file No.80-0020. It indicates that structure and phase of the host is not disturbed by doping and by the temperature variation and hence structural parameters like lattice parameter (a), micro strain (ε) and dislocation density are determined. An unknown peak at 81.03^0 appears in the XRD

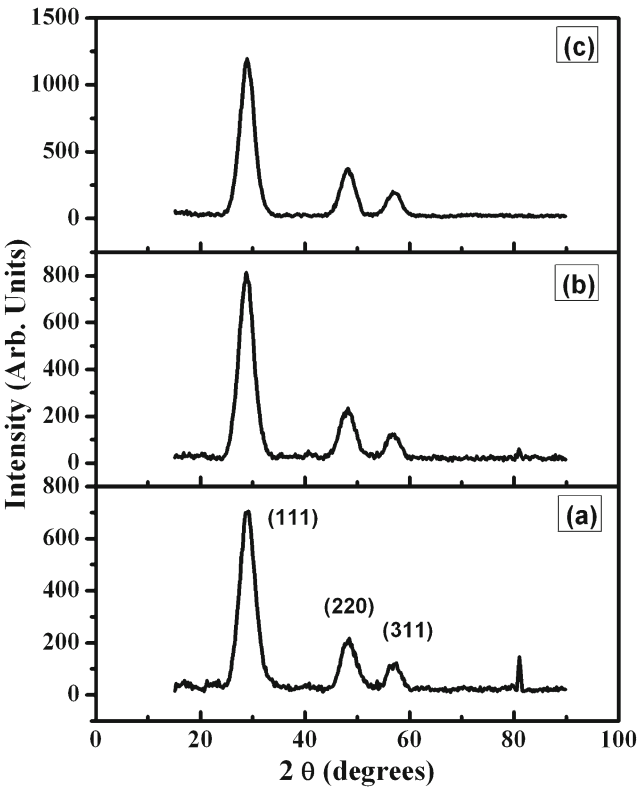

Fig. 1 XRD pattern of ZnS:Mn nanoparticles synthesized at (**a**) Room Temp, (**b**) 50 °C and (**c**) 70 °C

pattern of the sample prepared at room temp and at 50 °C which may be due to impurities. The intensity of peak decreases at 50 °C and disappears in the XRD for 70 °C. The intensity of XRD peaks slightly increases and the line-width decreases with the increase of synthesis temperature, suggesting the possibility of grain growth of ZnS: Mn2+ nanocyrstals. Average grain size (D) was calculated using the Debye–Scherer formula,

$$D = \frac{0.9\lambda}{\beta\cos\theta}$$

where β is the full width at half maximum (FWHM), θ is the Bragg angle and λ is the X-ray wavelength (0.15405 nm). Using above formula, the average grain size D of the ZnS:Mn^{2+}crystallites at room temperature, 50 and 70 °C are found to be 2.44, 2.53 & 2.61 nm respectively. Using the relation,

$$d_{hkl} = \frac{a}{\sqrt{(h^2 + k^2 + l^2)}}$$

the lattice parameters for prepared cubic ZnS: Mn^{2+} at the three temperatures were obtained as a=b=c=5.34, 5.35 & 5.33 Å. The corrected values of lattice constant are calculated from the Nelson–Riley plot. The N-R curve (Fig. 2) is plotted between the calculated 'a' for different planes and the error function (Nelson and Riley 1945).

$$f(\theta) = \frac{1}{2}\left(\cos^2\theta/\sin\theta + \cos^2\theta/\theta\right)$$

Y interception for the value of $f(\theta)=0$ gives the correct value of 'a'. The obtained values are 5.337, 5.34, &5.30 Å. This value is nearly similar to that of bulk ZnS which is 5.34 Å. Since ionic radii of Zn (0.74 Å) and Mn^{2+} (0.67 Å) are approximately same, no significant change in lattice parameter was seen due to the substitution of Mn^{2+} ions in ZnS lattice. Broadening of the peaks in the diffraction pattern indicates nano crystalline nature. According to this method, the FWHM (β) may be expressed as linear combination of lattice strain ξ and particle size (D) by the equation [22]:

$$\beta\cos\theta = \frac{0.9\lambda}{D} + \xi\sin\theta$$

Figure 3 shows the plot of β cos θ versus sin θ which is a straight line with slope ξ and intercept kλ/D. Putting the values of k and λ the crystallite size of Zns:Mn^{2+} nanoparticles at the three temperature are calculated as 2.47,2.52 &2.69 nm which are comparable to the calculated values by Scherer's equation. The strain of as prepared ZnS:Mn^{2+} nanoparticles is obtained from the slope and found to be 0.051, 0.021 & 0.017 at room temperature, 50 and 70 °C. Dislocations are defects in a crystal linked with disarray of the lattice in one part of the crystal with respect to another part. Unlike vacancies and interstitial atoms, dislocations are not equilibrium imperfections. In fact growth mechanism involving dislocation is a matter of importance. The dislocation density is given by the relation [23]

$$\delta = \frac{15\xi}{aD}$$

The dislocation densities of the three samples were estimated to be 5.8×10^{13}, 2.8×10^{13} and 1.8×10^{13} cm^{-2}. In polycrystalline samples dislocated atoms occupy the regions near the grain boundaries and their density is found to decrease with temperature. Using The ICP technique the actual Mn^{2+} concentration in the samples was determined by ICP-AES. The actual Mn concentration

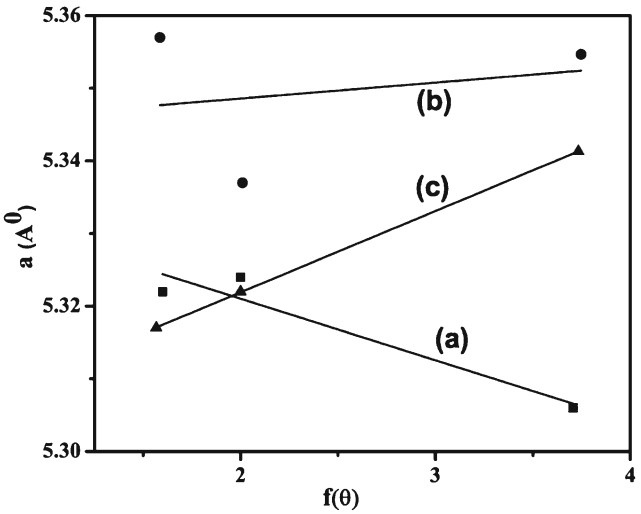

Fig. 2 N-R Plot of ZnS:Mn^{2+} nanoparticles synthesised at (**a**) RT, (**b**) 50 °C and (**c**) 70 °C

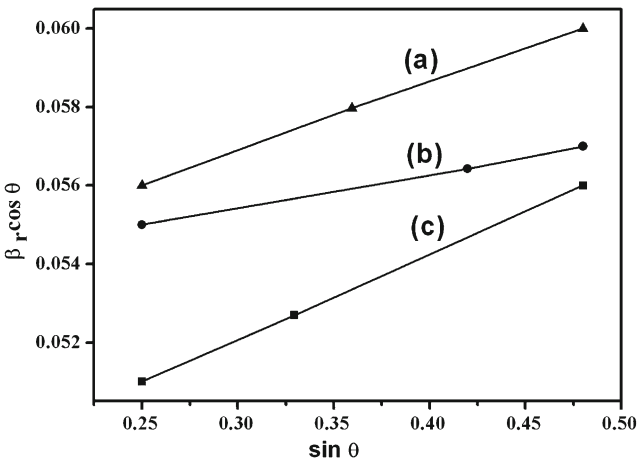

Fig. 3 β cos θ Vs sin θ of ZnS: Mn^{2+} nanoparticles synthesized at (**a**) RT, (**b**) 50 °C and (**c**) 70 °C

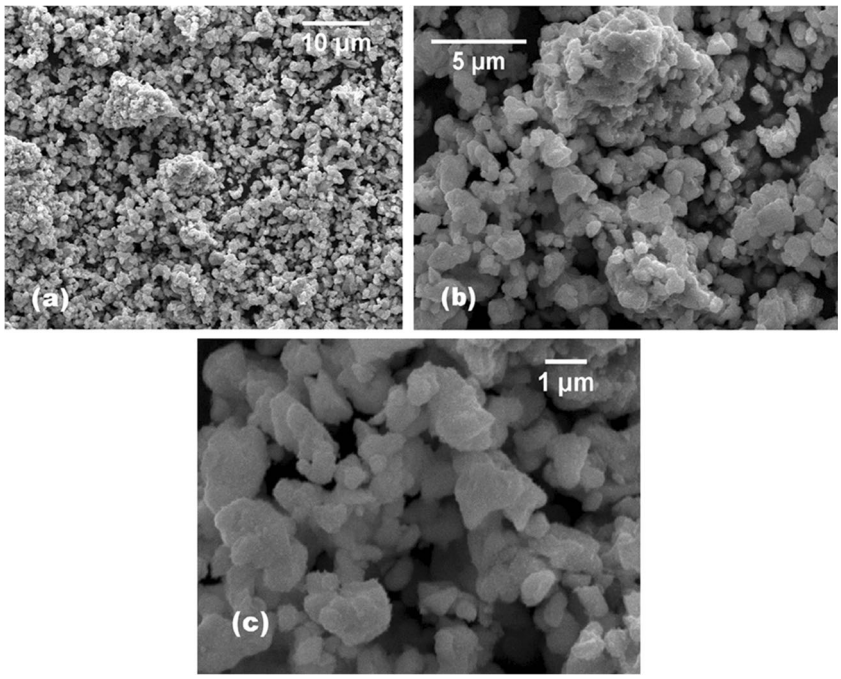

Fig. 4 SEM image ZnS: Mn^{2+} nanoparticles at (**a**) RT, (**b**) 50 °C and (**c**) 70 °C

in the ZnS:Mn samples were different from the Mn-precursor concentration (0.1 %M) being 0.05 %, 0.14 % and 0.17 % mol. % respectively for the samples at room temperature, 50 and 70 °C showing an increase with synthesis temperature which indicates better incorporation of Mn^{2+} in the crystal lattice.

SEM Study

SEM is a powerful tool to study the surface morphology especially by observing the top and the cross-sectional views. The morphological characterization (Fig. 4) revealed that the preparation temperature has an important role on the growth mechanism of the sample. The actual size of the nanoparticles cannot be determined from the SEM images as it is limited by the agglomeration of particles. The size of the building units (grains and clusters) is found to be increasing with temperature.

DRS and FTIR Studies

The diffuse reflectance spectra of ZnS:Mn^{2+} nanoparticles in the visible region are given in Fig. 5. The diffuse reflectance spectroscopy measurements confirm the blue shift in the bandgap of ZnS:Mn nanoparticles with respect to bulk

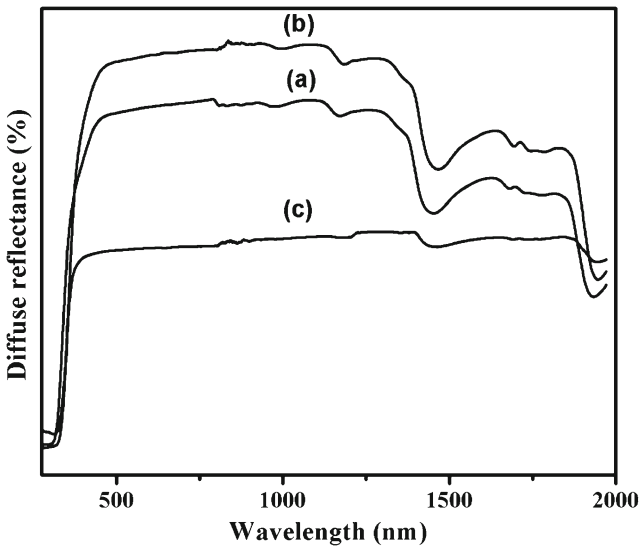

Fig. 5 Diffuse reflectance spectra of ZnS: Mn^{2+}nanoparticles at (**a**) RT, (**b**) 50 °C and (**c**) 70 °C

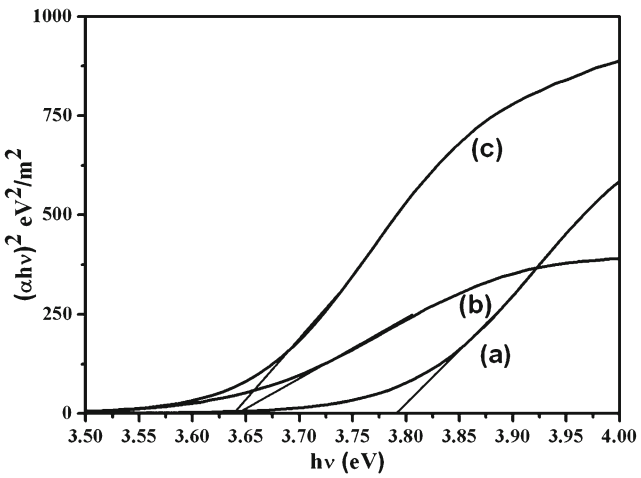

Fig. 6 $(\alpha h\nu)^2$ versus $(h\nu)$ of ZnS:Mn^{2+} at (**a**) RT, (**b**) 50 °C and (**c**) 70 °C

Table 1 Crystallite size, lattice parameter, strain, dislocation density & band gap of ZnS:Mn nanoparticles

Temperature	Crystallite size from Scherrer eqn. (nm)	Crystallite size from (W-H) method (nm)	Lattice parameter (Å)	Strain	Dislocation density$\times 10^{13}$ cm^{-2}	Band gap (eV)
Room Temperature	2.44	2.47	5.337	0.051	5.8	3.79
50 °C	2.53	2.52	5.34	0.021	2.8	3.65
70 °C	2.61	2.69	5.30	0.017	1.8	3.64

(3.65 eV). The absorbance was calculated from the reflectance using Kubelka-Munk equation [24, 25]. The bandgap, of the ZnS samples are estimated from the plot of $\{(k/s)\ h\nu\}^2$ vs $h\nu$ (Fig. 6) where k and s denote absorption and scattering coefficients and $h\nu$ is the photon energy. There is a red shift in the band gap with temperature which is due to the increase in particle size (Table 1).

Figure 7 shows room temperature FTIR spectra for the samples. The FTIR absorption peaks are the same for the three samples. The broad band between 2600 and 3700 cm^{-1} indicates the O-H stretching vibration of water molecules in the samples [26]. The peak at 1425 cm^{-1} is derived from the existence of C-O-H bending [26]. Peak at 2370 cm^{-1} is due to the C-O stretching mode [27]. Peaks at 664 and 447 cm^{-1} are due to the characteristic ZnS vibration [28]. The IR frequency along with the vibrational assignments of ZnS:Mn nanoparticles are given in Table 2.

Photoluminescence Study

We have measured room temperature PL spectra for the three samples at the same excitation wavelength of 340 nm (Fig. 8). It is found that the spectra consist of two broad bands with peak at 435 and 590 nm. The blue emission centred at 435 nm could be ascribed to a recombination of electrons at sulfur vacancy donor level with holes trapped at the zinc vacancy acceptor level [29]. The orange emission centred at 590 nm is attributed to the $^4T_1$–$^6A_1$ transition within 3d shell of Mn^{2+} ion [30]. It is also observed that at room temperature ZnS: Mn^{2+} nanoparticles emit blue light efficiently in comparison with orange emission. However, at 500C decrease in the intensity of blue emission and a slight enhancement in intensity of the yellow-orange emission are observed. But at 700C the blue emission and orange emission takes place in same level which demonstrates that the luminescence efficiency increases with temperature. The presence of efficient orange emission indicates that Mn^{2+} ions has been incorporated well into the ZnS nanoparticles which is consistant with ICP analysis. On the addition of Mn^{2+} ions in the ZnS lattice the Mn^{2+} ions replaces Zn^{2+} cation sites in ZnS lattice, hence the mixing of s–p electrons of host ZnS into the 3d electrons of Mn^{2+}causes powerful hybridization and the forbidden transition of $^4T_1$–$^6A_1$ becomes allowed, which yields orange emission at 590 nm [31, 32]. In order to realize the nature of the emission bands clearly, we have recorded room temperature photoluminescence excitation (PLE) spectra (Fig. 9) of ZnS: Mn2+ nanoparticles with λem at 590 nm. The PLE spectra of all samples involve one near band edge absorption centered at 340 nm (3.65 eV) and another absorption around 390 nm arising from the excitation to sublevels corresponding to intentionally incorperated Mn^{2+}. As dopant Mn ions create intermediate energy states below the excitonic states of ZnS nanocrystals, it was decided to assess the effect of synthesis temperature on the

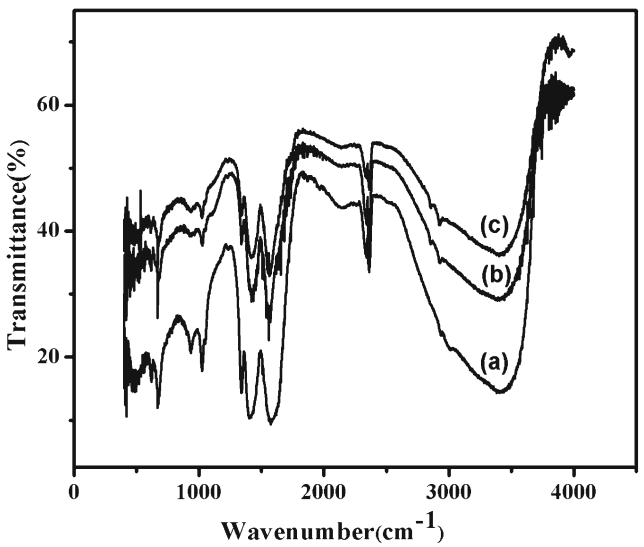

Fig. 7 FTIR Spectra ZnS:Mn nanoparticles (**a**) RT, (**b**) 50 °C (**c**) 70 °C

Table 2 Positions and vibrational assignments of ZnS:Mn nanoparticles

Wave number$\times 10^2$ m^{-1}	Assignment
447	Asymmetric bending
664	Symmetric bending
935	Asymmetric stretching
1045	Shoulder with asymmetric stretching
1425	C-O -H bending
1615	O-H bending
2370	C-O stretching
2600–3700	O-H stretching

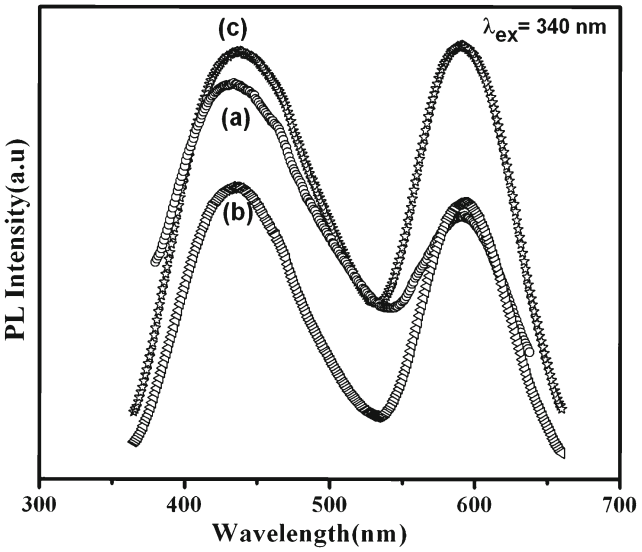

Fig. 8 Room Temp PL Spectra of ZnS: Mn^{2+} nanoparticles (**a**) RT (**b**) 50 °C (**c**) 70 °C

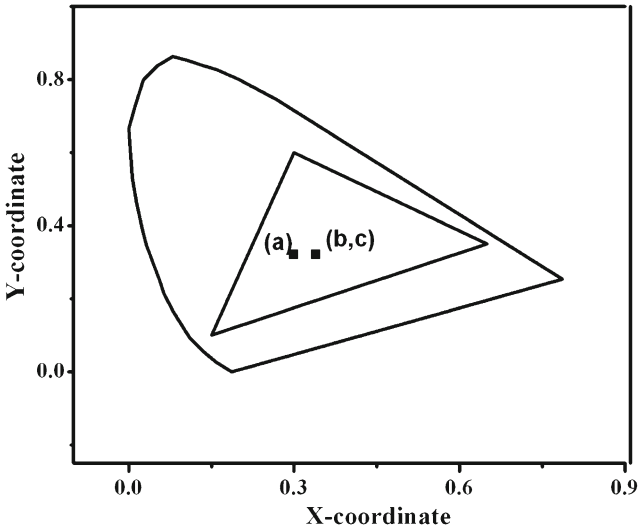

Fig. 10 CIE chromaticity diagram

luminescence properties of the ZnS:Mn^{2+} nanoparticles. The luminescence intensities were improved as the preparation temperature was increased from room temperature to 70 °C attributing enhanced crystallinity and better incorporation of Mn^{2+} in the crystal lattice.

To evaluate the effectiveness of ZnS:Mn nanoparticles to be used in light emitting devices, CIE (Commission International d'Eclairage 1931) chromaticity coordinates were calculated. The calculated colour coordinates are (0.30, 0.32), (0.34, 0.32) and (0.34, 0.32) and they are represented by the points (a), (b) & (c) in the chromaticity diagram (Fig. 10). Therefore, it can be assured that the characteristics of light emitted from all the three samples are in close agreement with achromatic white (x=0.33, y=0.33).

EPR Study

To obtain the oxidation state of manganese ions over the crystal lattice of the host, the synthesized sample at room temperature was analyzed by the EPR method. Since the host ZnS is not paramagnetic no EPR signal will be exhibited in its spectra [33]. The EPR spectra of ZnS:Mn^{2+} nanoparticles exhibited resonance signals at g=2.00 T with a six line hyperfine structure (Fig. 11) indicating the presence of the paramagnetic Mn^{2+} ions in the lattice. The hyperfine structure originates from the interaction between the Mn^{2+} electron clouds with its nuclei. This confirms the successful doping of paramagnetic Mn^{2+} ions in the ZnS crystal lattice.

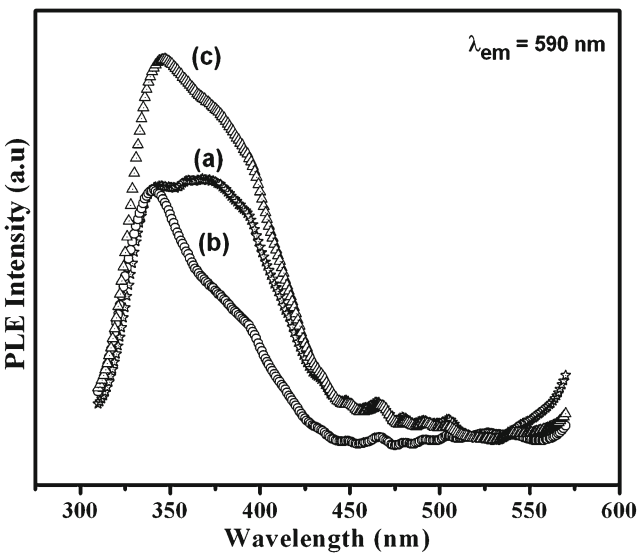

Fig. 9 Room Temp PLE Spectra of ZnS:Mn nanoparticles (**a**) RT, (**b**) 50 °C and (**c**) 70 °C

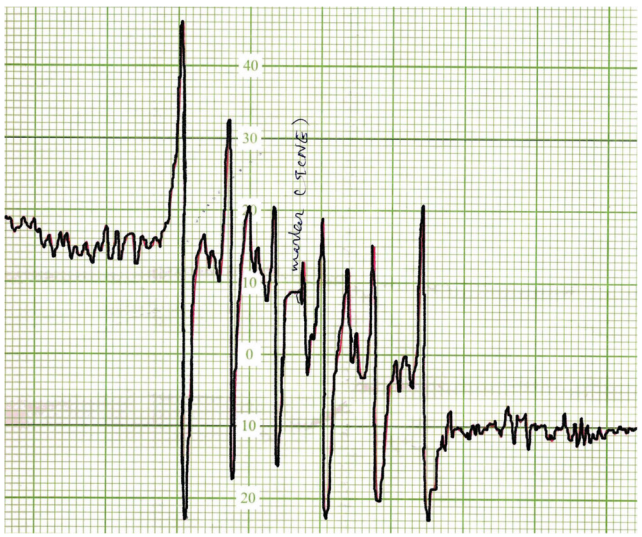

Fig. 11 EPR Spectra of ZnS: Mn^{2+}nanoparticles

Conclusion

Chemical Precipitation method was successfully used for the preparation of ZnS: Mn^{2+} nanoparticles at different temperatures. FTIR and X-ray diffraction can be used to classify the chemical bonding and crystal structure. The band gap of the ZnS:Mn^{2+} nanoparticles is red shifted with temperature which is due to the increase in particle size. The PL emission is white at all temperature with CIE co-ordinates in close agreement with achromatic white (x=0.33, y=0.33). EPR studies confirms the presence of Mn as Mn^{2+} in the ZnS lattice. Because of the white light emission, Zns:Mn nanophosphors may support simple device implementation and hold great assurance for the future of solid-state lighting.

Acknowledgments The authors would like to thank Department of Science and Technology, Govt. of India for financial support. KRB thank UGC for financial assistance through a minor project.

References

1. Pradhan N, Battaglia DM, Liu YC, Peng XG (2007) Nano Lett 7: 312–323
2. Dubertret B, Skourides P, Norris D, Noireaux JV, Brivanlou AH, Libchaber A (2002) Science 298:1759–1764
3. Pradhan N, Goorskey D, Thessing J, Peng XG (2005) J Am Chem Soc 127:17586–17598
4. Chan WCW, Nie S (1998) Science 281:2016–2023
5. Park W, Dim JM, YiG C, Bae MH, Lee H (2004) Appl Phys Lett 85:5052–5058
6. Archana NM, Ponnusamy S, Hayakawa Y, Muthamizhchelvan C (2009) Mater Lett 63:1931–1935
7. Igarashi T, Kusunoki T, Ohno T, Isobe K, Senna M (2001) Mater Res Bull 36:1317
8. Davies DA, Silver J, Vecht A, Marsh PJ, Rose JA (2001) J Electrochem Soc 48:H143
9. Karar N, Chander H, Shivaprasad SM (2004) Appl Phys Lett 85: 5058
10. Kim JP, Davidson MR, Puga-Lambers M, Lambers E, Holloway PH (2004) J Lumin 109:75
11. Peng WQ, Cong GW, Qu SC, Wang ZG (2006) Opt Mater 29:313
12. Jian C, Jinghai Y, Yonjun Z, Lili Y, Yaxin W, Maobin YL, Ming G, Xiaoyan L, Zhi X (2009) J Alloys Compd 486:890–894
13. Peng WQ, Qu SC, Cong GW, Zhang XQ, Wang ZG (2005) J Cryst Growth 282:179–185
14. Wenjin Z et al (2011) Inorg Chem 50:10432–10438
15. Le Donne A et al (2013) J Appl Phys 113:014903
16. Bol AA, Meijerink A (1998) Phys Rev B 58:R015997
17. Ding JX, Zapien JA, Chen WW, Lifshitz Y, Lee ST, Meng XM (2004) Appl Phys Lett 85:2361
18. Nanda J, Sarma DD (2001) J Appl Phys 90:2504
19. Xu SJ, Chua SJ, Liu B, Gan LM, Chew CH, Xu GQ (1998) Appl Phys Lett 73:478
20. Lü C, Cheng Y, Li UY, Liu F, Yang B (2006) Adv Mater (Weinheim, Ger) 18:1188
21. Bindu KR, Martinez AI, Vasudevan P, Unnikrishnan NV, Anila EI (2012) Phys E 46:21–24
22. Suryanarayana C, Grant Norton M (1998) X-ray diffraction: A Practical Approach. Plenum Press, New York
23. Nakamoto, Infrared Spectra of Inorganic and Coordination Compounds, Wiley, New York.
24. Kubelka P (1948) J Opt Soc Am 38:448
25. Kubelka P, Munk F (1931) Zh Tekh Fiz 12:593
26. Rita J, Sasi Florence S (2013) Mater Lett 107:93–95
27. Ummartyotin S, Bunnak N, Juntaro J, Sain M, Manuspiya H (2012) Solid State Sci 14:299–304
28. Zhang R, Liu Y, Sun S (2012) Opt Mater 34:788–1794
29. Ji-Won M, Ivanov IN, Joshi PC, Armstrong BL, Wang W, Jung H, Rondinone AJ, Jellison GE Jr, Meyer HM III, Jang GG, Meisner RA, Duty CE, Phelps TJ (2014) Acta Biomater 10:4474–4483
30. Kolmykov O, Coulon J, Lalevee J, Alem H, Medjahdi G, Schneider R (2014) Mater Sci Eng C 44:17–23
31. Remi B, Paul AI, Daniel Gamelin RJ (2008) Sol State Chem 18: 1582–1589
32. Sarkar R, Tiwary CS, Kumbhakar P, Basu S, Mitra AK (2008) Phys E 40:3115–3120
33. Amaranatha Reddy D, Sambasivam S, Murali G, Poornaprakash B, Vijayalakshmi RP, Aparna Y, Reddy BK, Rao JL (2012) J Alloys Compd 537:208–215